The FASEB Journal

RESEARCH ARTICLE

Biglycan stimulates retinal pathological angiogenesis via up-regulation of CXCL12 expression in pericytes

Miaomiao Liu[1] ⬤ | Peiquan Zhao[1] ⬤ | Huazhang Feng[1] ⬤ | Yuan Yang[1] | Xuerui Zhang[1] ⬤ | Enguang Chen[1] | Haodong Xiao[1] | Jia Luo[1] | Han Chen[1] | Jiawei Yin[1] | Min Lin[1] | Ruixue Mao[2] | Xingping Zhu[3] | Jing Li[1] | Ping Fei[1] ⬤

[1]Department of Ophthalmology, Xinhua Hospital Affiliated to Shanghai Jiao Tong University School of Medicine, Shanghai, China

[2]Naval Healthcare Information Center, PLA Naval Medical University, Shanghai, China

[3]Department of Ophthalmology, Xinhua Hospital Affiliated to Shanghai Jiao Tong University School of Medicine, Changxing Branch, Shanghai, China

Correspondence
Ping Fei and Jing Li, Department of Ophthalmology, Xinhua Hospital Affiliated to Shanghai Jiao Tong University School of Medicine, Shanghai, China.
Email: shirleypingfei@126.com; feiping@xinhuamed.com.cn and lijing@xinhuamed.com.cn

Abstract

Retinal pathological angiogenesis (PA) is a common hallmark in proliferative retinopathies, including age-related macular degeneration (AMD), proliferative diabetic retinopathy (PDR), and retinopathy of prematurity (ROP). The mechanisms underlying PA is complex and incompletely understood. In this study, we investigated the role of extracellular matrix (ECM) protein biglycan (BGN) in PA using an oxygen-induced retinopathy (OIR) mouse model, along with hypoxia (1% O_2) conditions for incubating pericytes and endothelial cells in vitro. We found a significant upregulation of *Bgn* in the retinas of OIR mice. Intravitreal injection of *Bgn*-specific small interfering RNA (siRNA) in OIR mice at postnatal day 12 (P12) effectively curbed retinal PA at P17. Using cultured cells, we found that *BGN* expression in pericytes was highly sensitive to hypoxic stimulation compared to endothelial cells. We further showed that BGN stimulated retinal PA via the upregulation of C-X-C motif chemokine ligand 12 (CXCL12). Inhibition of the CXCL12-CXCR4 axis effectively diminished PA in OIR mouse. In conclusion, our study demonstrated the stimulatory role of BGN in retinal PA, identified the

Abbreviations: AMD, age-related macular degeneration; ANGPTLs, angiopoietin-like proteins; BGN, biglycan; CM, culture media; CXCL12, C-X-C motif chemokine ligand 12; DAMP, danger-associated molecular pattern; DAPI, 4′,6-diamidino-2-phenylindole; DEGs, differentially expressed gene; E18, embryonic day 18; ECM, Extracellular matrix; GEO, Gene Expression Omnibus; GO, Gene Ontology; H&E, Hematoxylin and eosin; HRMEC, human retinal microvascular endothelialcell; HRMVPC, human retinal microvascular pericyte cell; hrs, hours; NV, neovascular; OIR, oxygen-induced retinopathy; P12, postnatal day 12; PA, pathological angiogenesis; PCs, Pericytes; PDR, proliferative diabetic retinopathy; ROP, retinopathy of prematurity; ROS, reactive oxygen species; siRNA, small interfering RNA; SLRP, small leucine-rich repeat proteoglycan; TLR, toll-like receptors; VEGF, vascular endothelial growth factor; VO, vessel obliteration.

Miaomiao Liu and Peiquan Zhao should be considered joint first authors.

Ping Fei (lead contact) and Jing Li should be considered joint senior authors.

---

link between BGN and CXCL12 expression, and further highlighted the role of pericytes in retinal PA.

1 | INTRODUCTION

Pathological angiogenesis (PA) is one of the common pathological changes underlying proliferative retinopathies, encompassing the wet form of age-related macular degeneration (AMD), proliferative diabetic retinopathy (PDR), and retinopathy of prematurity (ROP).[1–3] In these conditions, the structural integrity and retinal perfusion function of the pathological blood vessels are compromised, rendering it vulnerable to vitreous hemorrhage and macular edema, and ultimately, culminates in visual impairment, or even complete vision loss.[4–6] While intraocular injection of anti-vascular endothelial growth factor (VEGF) agents is effective in controlling leaky vasculature, its long-term effect on vascular regression is far from ideal.[7–10] Hence, there is a pressing need for more effective therapies to control the occurrence of pathological intraocular angiogenesis.

Extracellular matrix (ECM) plays important role in modulating tissue homeostasis. Previously, we have shown that various ECM proteins affected the growth and function of the retinal blood vessel.[11–14] Biglycan (BGN) is a member of small leucine-rich repeat proteoglycan (SLRP) family, and is found in the ECM of various tissues, including retina.[15,16] In human eyes, it is presented in all layers of the neural retina tissue, as well as in Bruch's membrane, choroid, sclera, and choroidal vessels.[17] Studies in mice showed that BGN can be detected in the retina and optic nerve by embryonic day 18 (E18) and showed intense staining in synapse-rich layers by postnatal day 42 (P42).[18] BGN is a danger-associated molecular pattern (DAMP) protein which binds to toll-like receptors (TLR) and induces proinflammatory responses.[19–21] BGN is synthesized by many cell types, including endothelial cells, smooth muscle cells, fibroblasts, and macrophages.[22] In situations of tissue injury or stress, BGN is either proteolytically cleaved or newly synthesized into its soluble form.[15,23,24] Soluble BGN is involved in many physiological and pathological conditions, including bone formation, cancer development, hepatic fibrosis, and adaptive remodeling after myocardial infarction.[25–30] A growing body of evidence, both in neoplastic and non-neoplastic contexts, suggests that BGN plays a role in angiogenesis by regulating the expression of VEGF, endostatin, and angiopoietin-like proteins (ANGPTLs).[16,31–34] However, studies investigating the role of BGN on retinal neovascularization are limited. Recent findings have indicated increased BGN cleavage products in the vitreous of proliferative diabetic retinopathy (PDR) patients,[35] highlighting its potential involvement in retinal PA.

Pericytes (PCs) have emerged as promising targets for anti-angiogenic therapy.[36–38] Located within the capillary basement membrane, pericytes closely interact with endothelial cells and play a crucial role in regulating blood flow, immune responses, and microvessel physiology through factors like VEGF, PDGFB, Notch, and TGF-β.[39–41] They are vulnerable to injury from hypoxia, oxidative stress, and inflammation, leading to disrupted communication with endothelial cells and microvascular dysfunction under these stresses.[42–44] Most studies on pericyte biology focus on compromised recruitment or development, there are several research on the specific pathophysiological changes in pericytes and their effects on retinal pathological angiogenesis, particularly regarding their paracrine interactions with endothelial cells.[45–48] Thus, further investigation is needed to clarify the mechanisms of pericyte function in this context to develop effective preventive strategies.

In this study, we employed the oxygen-induced retinopathy (OIR) mouse model to investigate the role of BGN on retinal PA. Silencing the expression of *Bgn* via *Bgn*-specific small interfering RNA (siRNA) could effectively curb the pathological neovascularization in OIR mice. Our findings also suggest that *BGN* expression in pericytes is sensitive to hypoxic conditions in vitro. Furthermore, we showed that the pro-angiogenic effect of BGN was largely mediated by increased production of C-X-C motif chemokine ligand 12 (CXCL12).

2 | METHODS

2.1 | Animals and treatments

All experiments in this study were conducted following the guidelines of the Association for Research in Vision and Ophthalmology Statement for the Use of Animals in Ophthalmic and Vision Research and approved by the

Institutional Animal Care and Use Committee of Xinhua Hospital Affiliated to Shanghai Jiao Tong University School of Medicine. Time-pregnant female C57BL/6 mice were purchased from the Shanghai Laboratory Animal Center, Chinese Academy of Sciences (Shanghai, China). All mice had unrestricted access to food and water. To induce PA in the OIR model, the P7 C57BL/6J puppies were exposed to 75% oxygen for 5 days, accompanied by lactating mother mice. Subsequently, the mice were returned to room air (RA) environment (from the age of P12 to P17). Age-matched littermate control mice were maintained in RA environment throughout the entire period. The mother mice of the OIR group and control group were alternated every 12 h (hrs).

Unless otherwise specified, all treatment intervention were performed on P12 mice, right after they were transferred out of the hyperoxic chamber. The pupils were dilated with 0.5% tropicamide. One microliter of *Bgn*-specific siRNAs (1 nmol/μL), LIT927 (250 ng/μL), IT1t (500 ng/μL) or PBS was injected into the vitreous cavity using a 2.5-μL Hamilton syringe with a 32-gauge needle (Hamilton, NV, USA). All mice were sacrificed by CO_2 euthanasia at P17. Eyes were immediately enucleated and processed accordingly as needed.

2.2 | Immunohistochemistry

Retinal whole mount and immunofluorescent staining of the cells and frozen section were carried out as previously described.[12,49] QuickBlock blocking buffer (Beyotime, China) was used for 30 min at room temperature. The following primary antibodies: isolectin B4 conjugated with Alexa Fluor 488 (1:200; Invitrogen antibodies), rabbit anti-BGN (Proteintech, #16409-1-AP, 1:100), rabbit anti-CXCL12 (Boster, #BA1389, 1:200), rabbit anti-hypoxia inducible factor 1, alpha subunit (HIF-1a) (Abcam, #AB179483, 1:100), and mouse anti-chondroitin sulfate proteoglycan 4 (NG2) (Merck, #MAB5384, 1:200) were used and incubated overnight at 4°C. Alexa Fluor-488- or 568-conjugated secondary antibodies purchased from ThermoFisher were used. Finally, the slides were sealed with an antifade reagent containing 4′,6-diamidino-2-phenylindole (DAPI) (ThermoFisher, #S36938).

Stained retinal tissues were imaged using either fluorescent microscopy (Olympus BX51) or confocal microscopy (Leica TCS SP8). Hematoxylin and eosin (H&E) stained retinal sections were imaged using light microscopy. To determine the neovascular (NV) and vessel obliteration (VO) areas of the retina, the polygon lasso tool and magic wand of Adobe Photoshop 2022 (San Jose, CA, USA) were used. The avascular region and neovascularization were quantitatively determined as the percentage of pixels in relation to the entire retina.

2.3 | Cell culture and treatment

The human retinal microvascular pericyte cell (HRMVPC) and human retinal microvascular endothelial cell (HRMEC) were purchased from Anwei-sci Cell Center (Shanghai, China, #H0773, #H0774). HRMVPCs were cultured in high-glucose DMEM supplemented with 10% fetal bovine serum (FBS) and 1% penicillin/streptomycin. HRMECs were cultured in endothelial medium supplemented with 10% FBS and 1% penicillin/streptomycin. All cell culture reagents were purchased from ThermoFisher unless otherwise specified. The cells were maintained at 37°C in a humidified incubator with 5% CO_2. To establish an in vitro hypoxia model, the cells were cultured in a humidified incubator with 1% O_2 for 24 or 48 h as specified.

For proliferation analysis, a 5-ethynyl-2′-deoxyuridine (EdU) labeling kit was purchased from Beyotime (Shanghai, China, C0078s) and used according to the manufacturer's instruction.

For the determination of intracellular reactive oxygen species (ROS) level, HRMVPCs were plated on the precoated coverslip in 12-well plates and treated as needed. Serum-free fresh medium containing 2 μM dihydroethidium (DHE) (Beyotime, Shanghai, China) were used to incubate the cells for 30 mins in the dark. The coverslips were then imaged under fluorescent microscope (Olympus BX51) with 532 nm excitation laser and a 580 nm long-pass detection filter. The intensity of the fluorescence of the entire section was quantified using ImageJ and used for comparison between groups.

For migration analysis, 4×10^5 HRMECs or HRMVPCs were seeded in 6-well plates. They were then treated accordingly as needed. A uniform scratch was created by scraping with the tip of a 1 mL pipette. The cells were then cultured for 36 (HRMVPCs) or 48 h (HRMECs). Images of the gap were taken immediately after scratching and before the termination of the experiment. The migration rate was determined by quantifying the area repopulated with cells within the original gap.

For endothelial cell tube formation analysis, 100 μL/well of Matrigel (Corning, Shanghai, China, #354230) was plated into 48-well plate and incubated for 1 hour at 37°C. HRMECs between passages 3 and 5 were plated on Matrigel at a density of 5×10^4 cells per well. Images were captured 6 h after incubation to evaluate the formation of tubular structures.

For CXCL12 reintroduction experiments, recombinant human CXCL12 protein (MedChemExoress, Shanghai, China, #HY-P700642, 200 ng/mL) was applied.
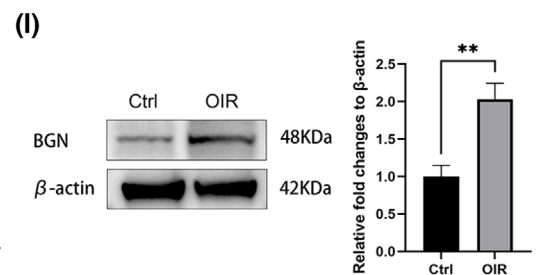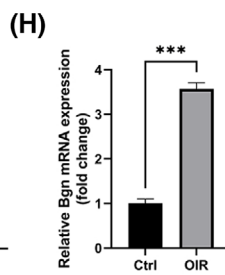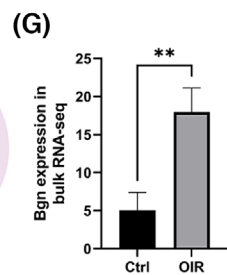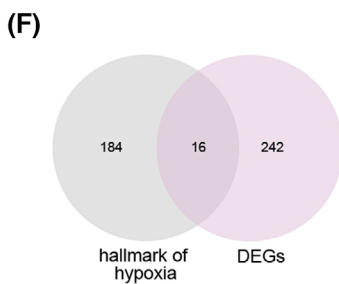
(A)

(B)

(C)

(D)

(E)

(F)

(G)

(H)

(I)
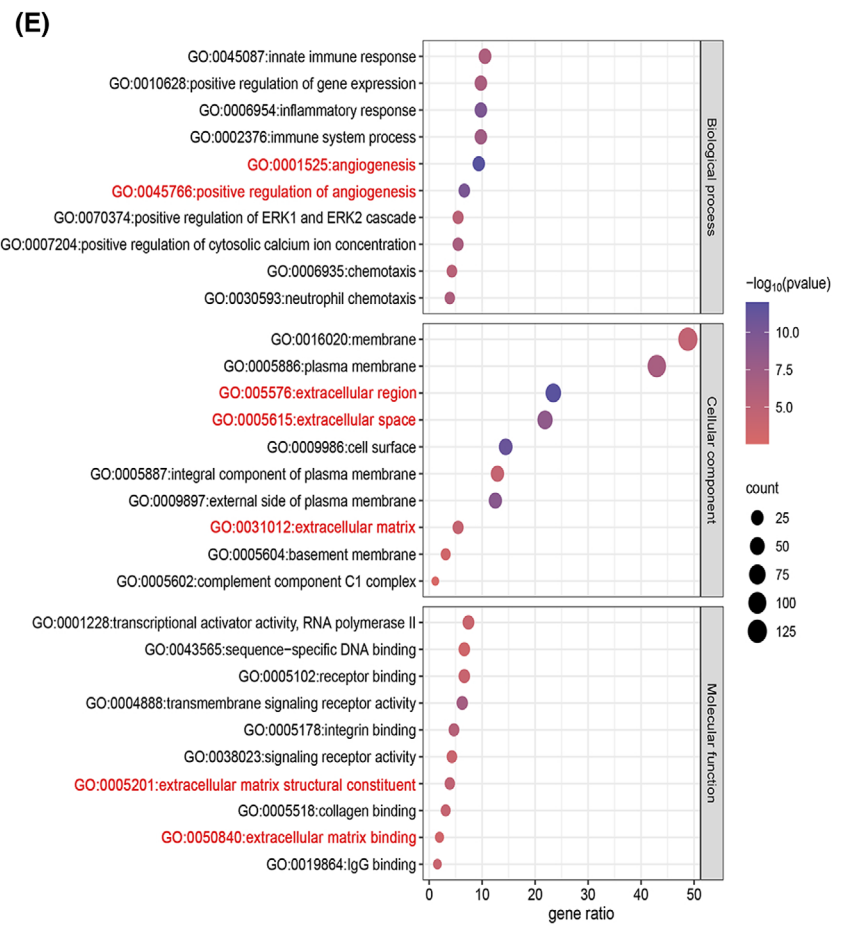
FIGURE 1 BGN is upregulated during pathological angiogenesis. (A) Schematic diagram of the mouse OIR model. Pups were exposed to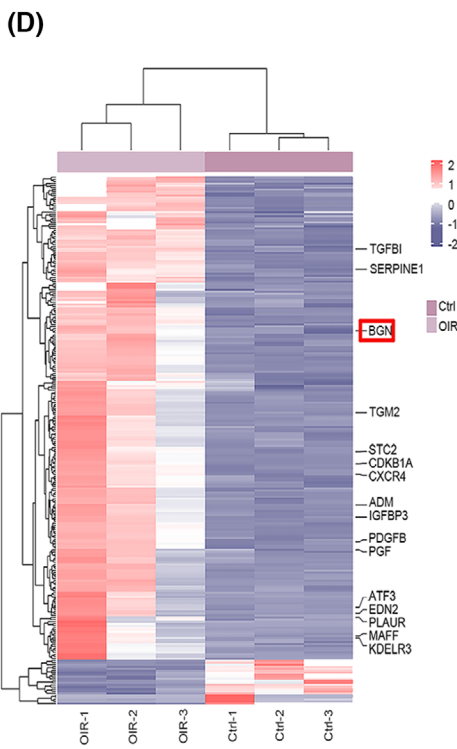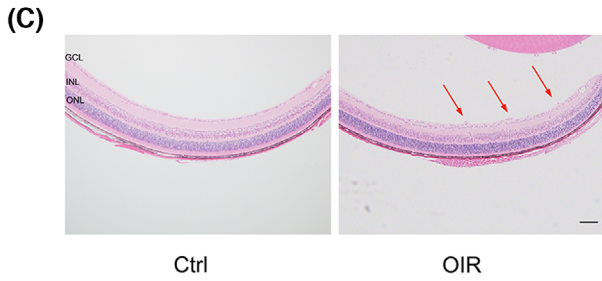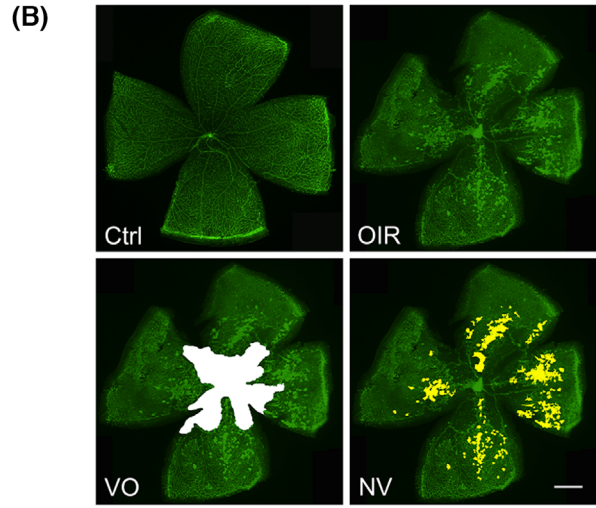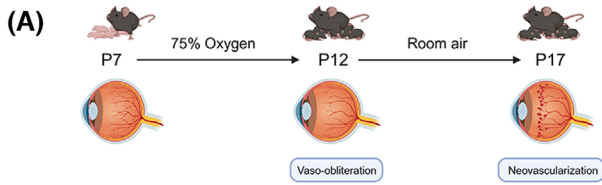 75% oxygen from P7 to P12 and returned to normoxia from P12 to P17, while control mice remained in normoxic environment throughout the entire period. Retinal neovascularization peaked at P17 in OIR mouse. (B) Representative images of flat-mounted retinas stained with IB4 (green) showing blood vessels in control and OIR mice at P17. Vaso-obliteration (VO) and neovascular (NV) areas in OIR mice are delineated in white and yellow respectively. (C) Representative images of H&E staining of control and OIR retinal sections at P17. Red arrows indicate the retinal neovascularization which projects to the vitreous cavity. Scale bar: 100 μm. (D) Heatmap of 258 DEGs between control and OIR retinas at P17. The 16 genes which are also "hallmark of hypoxia" genes, including *BGN* in red rectangle, are labeled. (E) The top 10 GO terms relate to biological process, cellular component, and molecular function enriched by 258 DEGs. Terms related to neovascularization and ECM are labeled in red. (F) Venn diagram shows the 16 overlapped genes between 258 DEGs and 200 "hallmark of hypoxia" genes listed in the Molecular Signatures Database (MSigDB). The gene symbols are given in figure D. (G) *Bgn* expression in Bulk RNA-sequencing data between control and OIR retinas at P17. (H) *Bgn* expression in retinas from P17 control and OIR mice. The expression in control retina is set as 1. The experiments were repeated using retinal samples taken from six different animals in the OIR group and three different animals in the control group. (I) Western blot analysis of retinal BGN expression in control and OIR mice at P17. The density of the bands was quantified using ImageJ and β-actin was used as internal control. The experiments were repeated using four different retinal total lysates in each group, and the quantification of the result was presented at right.

2.4 | RNA interference

For in vivo knockdown of BGN expression, we designed specific small interfering RNA (siRNA) targeting *Bgn* cDNA (GeneBank accession no. NM_001411776.1), the primer sequences were 5′-GGCCAUCCAAUUUGGAAAUTT-3′ (forward primer) and 5′-AUUUCCAAAUUGGAUGGCCTT-3′ (Shanghai, GenePharma Co. Ltd., China). Control siRNA sequences were as follows: 5′-UUCUCCGAACGUGUCACGUTT-3′ (forward primer) and 5′-ACGUGACACGUU CGGAG AATT-3′. The siRNAs were modified at the 3′ end with 2-o-methylation to be protected from degradation. The transfection efficiency was assessed by real-time PCR and Western blotting.

For in vitro knockdown of BGN expression, we designed siRNA targeting *BGN* cDNA (GeneBank accession no. NM_001711.6), the primer sequences were 5′-CCAUCCAGUUUGGCAACUATT-3′ (forward primer) and 5′-UAGUUGCCAAACUGGAUGGTT-3′ (Shanghai, GenePharma Co. Ltd., China). Control siRNA sequences were as follows: 5′-CCAUCCAGUUUGGCAACUATT-3′ (forward primer) and 5′-UAGUUGCCAAACUGGAUGGTT-3′. Transfections were performed with siRNA or negative controls using Lipofectamine 3000 from Invitrogen according to the manufacturer's instructions.

## 2.5 | Western blot and Enzyme-linked immunosorbent assay (ELISA) analysis

For Western blot analysis, the retinal tissues and cultured cells were lysed in radioimmunoprecipitation assay (RIPA) buffer supplemented with Phenylmethanesulfonyl fluoride PMSF (Yeasen, Shanghai, China, #20104ES08) and protease and phosphatase inhibitor mini tablets (Beyotime, Shanghai,

China). After centrifugation at 75 000*g* for 10 min at 4°C, the supernatant was collected, and protein concentration was determined using a BCA assay kit (Epizyme, China). Subsequently, equal amount of each protein sample was loaded onto SDS–PAGE gels and transferred to PVDF membranes (Immobilon-P; Millipore, Schaffhausen). The following antibodies were used: rabbit anti-BGN (Proteintech, #16409-1-AP, 1:1000), rabbit anti-CXCL12 (Abcam, #AB155090, 1:1000), rabbit anti-HIF-1a (Abcam, #AB179483, 1:1000), rabbit anti β-actin (Abclonal, #AC026, 1:2000), and incubated overnight at 4°C. The corresponding horseradish-conjugated secondary antibody was used in conjunction of enhanced chemiluminescence (ECL) reagent for the visualization of the proteins by ChemiDoc imaging system (Bio-Rad). The intensity of the bands was quantified and calculated. β-actin was used as loading control.

BGN and CXCL12 concentrations in the cell culture medium were measured using commercial ELISA kits (Elabscience, China, #E-EL-H6091; Elabscience, China, #E-EL-H0052c) according to the manufacturer's instruction.

2.6 | RNA isolation and real-time PCR assays

Total RNA was extracted utilizing an RNA extraction kit (B0004DP; EZBioscience). Subsequently, 1 μg of each RNA sample were used for cDNA synthesis using PrimeScript™ RT (Takara, Japan) following the manufacturer's instructions. Quantitative real-time PCR analysis was carried out using TB Green® Premix Ex Taq™ II (Takara, Japan). The gene expression levels relative to β-actin were calculated using the $2^{-\Delta\Delta Ct}$ method. The primer sequences were as follows: mouse *Bgn*, 5′-GACAACCGTATCCGCAAAGT-3′ (forward primer) and 5′-CAAAGGCTCCTGGTTCAAAG-3′
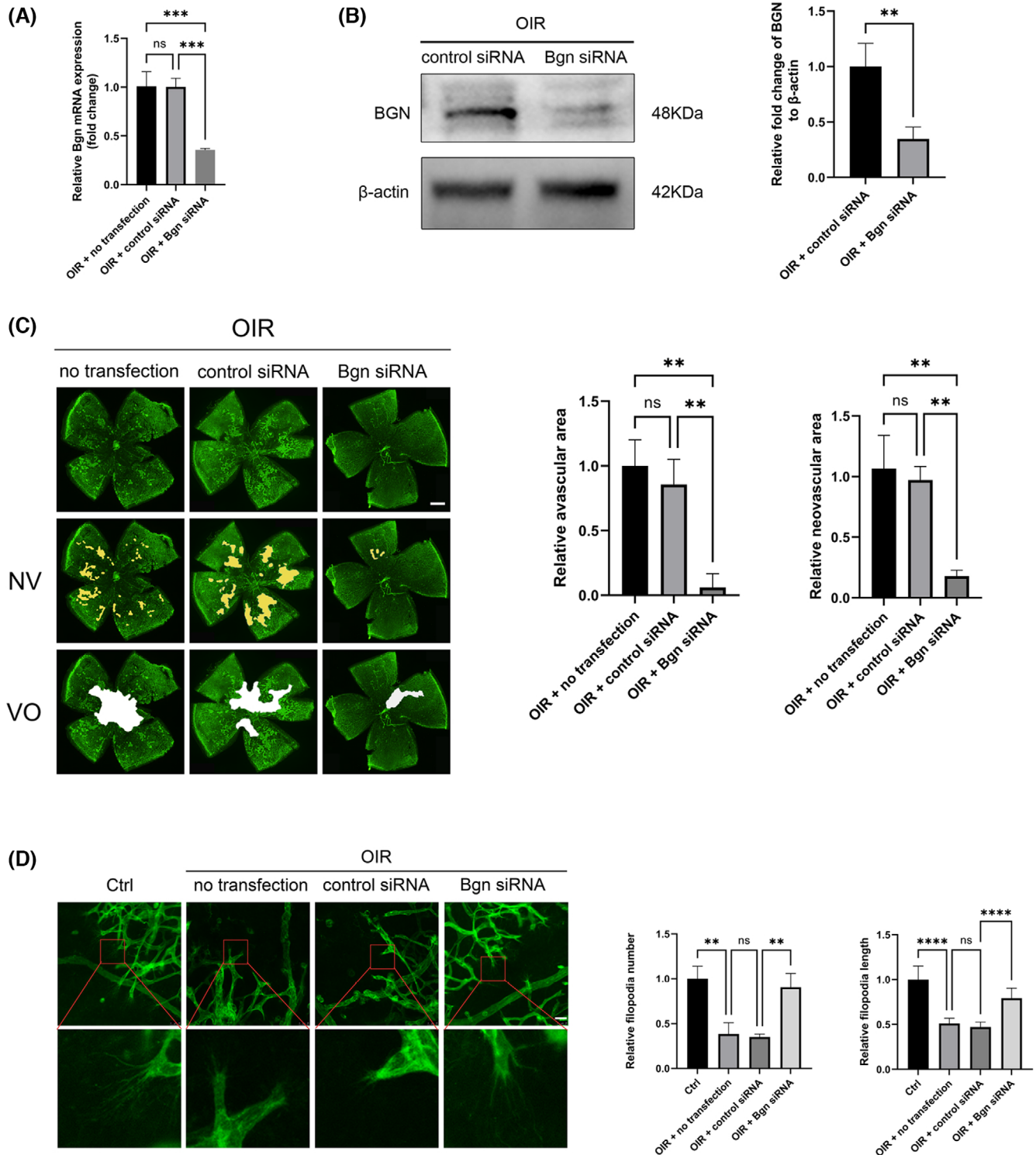
(reverse primer); human *BGN*, 5′-CAAGCTCCTCCAGGTG GTCTA-3′ (forward primer) and 5′-TGAAGAGGCT GATGCCGTTG-3′ (reverse primer); mouse *Actb*, 5′-CACTGTCGAGTCGCGTCC-3′ (forward primer), and 5′-TCATCCATGGCGAACTGGTG-3′ (reverse primer); human *ACTB*, 5′-CATGTACGTTGCTATCCAGGC-3′ (forward primer) and 5′-CTCCTTAATGTCACGCACGAT-3′ (reverse primer).

2.7 | RNA sequencing and data analysis

The transcriptional profiles of the mouse retina and human HRMVPC were generated using bulk RNA-sequencing (OEbiotech and Novogene Corporation, Inc), respectively. Intergroup differentially expressed gene (DEGs) was screened by Limma package in R, and |Fold change| >1.5 and adjusted p-value <.01 were

FIGURE 2 BGN deficiency alleviates retinal pathological angiogenesis. (A) qPCR analysis of *Bgn* expression in the retina of P13 OIR mice subjected to *Bgn*-specific siRNA treatment. One microliter of siRNA (control siRNA, non-specific scribble RNA; *Bgn* siRNA, *Bgn*-specific targeting siRNA) was injected intravitreally on P12 and the retinal tissues were harvested 24 h later for RNA extraction and qPCR analysis. The expression of *Bgn* in no transfection retinas was set as 1. The experiments were repeated using six different retinal samples in each group and the average relative expression is presented. (B) Western blot analysis of BGN protein in P17 OIR retinas treated with control siRNA and *Bgn* siRNA. The density of the bands was quantified using ImageJ and β-actin was used as internal control. The experiments were repeated on five different retinal total lysates in each group. The average result is presented at the right. (C) Immunofluorescent staining of IB4 on whole-mount P17 retinal samples pretreated with control siRNA or *Bgn* siRNA on day P12 as described above. The NV area is marked in yellow, and the VO area is marked in white. The staining was performed on 10 retinas of *Bgn* siRNA group and five retinas of control group and the average results is presented at the right. Scale bar: 500 μm. (D) Vascular sprouting (distal sprouts and filopodia) of the P17 retina of control, OIR, OIR treated with control siRNA, and OIR treated with *Bgn* siRNA. The whole mount retina was stained with IB4 (green). The average length and number of filopodia are quantified (right). The staining was performed on four different retinal samples from each group. Data are expressed as mean ± SD (*t* test). ns, not significant. **$p < .01$; ***$p < .001$; ****$p < .0001$. Scale bar: 25 μm.

considered as threshold between OIR and control mice. |Fold change| >0.5 and adjusted *p*-value <.05 were considered as threshold between HRMVPC groups. The functional enrichment analysis was performed using DAVID tool. Venn diagram analysis was used for the extraction of overlapped genes.

Additionally, bulk RNA-sequencing data (GSE102485) from the Gene Expression Omnibus (GEO) were analyzed. This dataset contained RNA sequencing results obtained from 20 human neovascular proliferative membranes of PDR patients and three control samples without PDR. The DEGs were identified using the threshold of |Fold change| >1.0 and adjusted *p*-value <.05.

2.8 | Statistical analysis

To evaluate the normality of the data, the Shapiro–Wilk test was employed. For normally distributed data, unpaired Student's *t*-test was utilized to compare the means between groups. Two-way analysis of variance (ANOVA) was applied for experiments involving multiple groups. Data were processed using GraphPad Prism 9.0 and are expressed as mean ± standard deviation (SD), with a minimum of three independent experiments conducted. The differences with $p < .05$ was considered statistically significant.

3 | RESULTS

3.1 | BGN is upregulated during pathological angiogenesis

The OIR model is a well-established system to study retinal PA.[50,51] In this model, neonatal mice are exposed to 75% oxygen from P7 to P12, causing the regression of immature retinal vessels.[50] This is followed by exposure to RA from P12 and P17, which is characterized by PA

at the junction between avascular and vascularized retina.[50] Normally, the PA peaks at P17 (Figure 1A). The distinct avascular and neovascular areas were seen with IB4 staining of the retinal whole mount (Figure 1B), and the pathological neovascularization protruding into the vitreous cavity was evident in H&E staining of the retinal sections (Figure 1C). We compared retinal gene expression profiles of OIR-treated and RA-raised mice at P17 and found 258 DEGs (Figure 1D). Gene ontology (GO) analysis of the DEGs showed that many terms related to neovascularization and ECM were significantly enriched (Figure 1E). Given the critical role of hypoxia in the OIR model, we compared our list of DEGs with 200 hallmarks of hypoxia-responsive-genes from the Molecular Signatures Database (MSigDB), and found 16 genes in common (Figure 1F). Of particular interest, BGN, a member of SLRP family ubiquitously exists in ECM, exhibited a remarkable 3.43-fold increase in the OIR retina (Figure 1G). The increased expression of *BGN* was also confirmed by real-time PCR analysis (Figure 1H), Western blot analysis (Figure 1 I) and immunofluorescent staining of retinal sections (Figure S1) using a separate set of RA- and OIR-treated retinal RNA samples. Together, these findings confirmed the upregulation of BGN in the OIR retina.

3.2 | BGN deficiency alleviates retinal pathological angiogenesis

To investigate the role of BGN in retinal PA, we reduced *Bgn* expression in the mouse retina by intravitreal injection of *Bgn*-specific targeting siRNA. When injected on P12, the *Bgn* siRNA effectively reduced BGN expression in the retina at both the mRNA and protein levels (Figure 2A,B). *Bgn* siRNA treatment also effectively decreased the avascular and neovascular areas in OIR mice when analyzed on P17 (Figure 2C), while no significant change was observed in the RA-raised control group at the same age (Figure S2). H&E staining
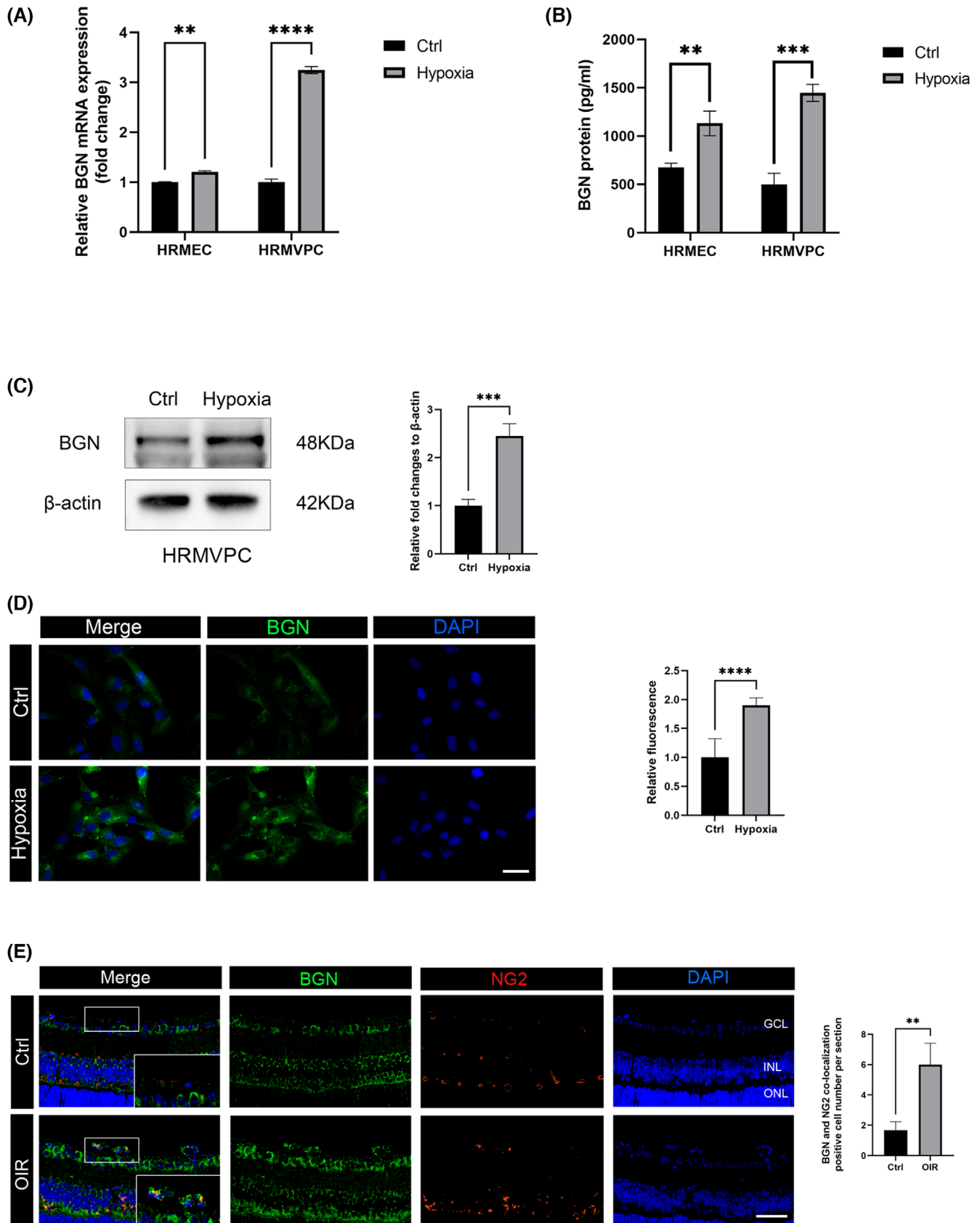
demonstrated a significant reduction in neovascular protrusion into the vitreous cavity in *Bgn* siRNA-treated OIR mice (Figure S3). The onset of PA coincides with the cessation of normal vascular sprouting in the OIR model. Interestingly, *Bgn* siRNA treatment reversed the inhibitory effect of normal retinal angiogenesis in OIR model (Figure 2D). Collectively,

FIGURE 3 BGN expression in pericytes is highly sensitive to hypoxic conditions. (A) *BGN* expression in HRMECs and HRMVPCs cultured under normoxic and hypoxic conditions (1% O_2 for 24 h). *BGN* expression under normoxic condition was set as 1 for each cell type. The experiments were repeated six times for each cell type under each condition and the average expression is presented. (B) BGN protein level in the supernatant of HRMECs and HRMVPCs cultured under above groups. The experiment was repeated in three different samples of each group. (C) Western blot analysis of BGN in HRMVPCs after hypoxia treatment for 24 h. Right panel shows the quantification results of densitometric analysis. β-actin was used as loading control. The experiment was repeated in 6 different samples of each group. (D) Immunofluorescent staining of BGN (green) in HRMVPCs after hypoxia treatment for 24 h. The nuclei were stained with DAPI (blue). The experiment was repeated in four different samples of each group. The images were taken under the same exposure conditions and the fluorescent signals of BGN were quantified using ImageJ (right). Scale bar, 50 μm. (E) Co-immunofluorescent staining of BGN (green) and NG2 (red), a marker for pericytes, in P17 retinal cross sections of control and OIR mice. The area within the white rectangles is magnified and presented at the bottom right, showing the co-localization of BGN and NG2 in the retina of OIR. Quantification of BGN fluorescence signal colocalized with NG2. Data are expressed as mean ± SD (*t* test). Scale bar: 50 μm. ns, not significant. ***p* < .01; ****p* < .001; *****p* < .0001.

these findings suggested that inhibition of BGN expression alleviated retinal PA and promoted normal revascularization.

3.3 | BGN expression in pericytes is highly sensitive to hypoxia conditions

Next, we compared *BGN* expression in cultured HRMEC and HRMVPC, two types of cells which are most closely associated with retinal angiogenesis.[39,52] Increased expression of *BGN* was found in both cells in response to hypoxia. However, a higher fold of increase was observed in HRMVPCs compared to HRMECs in both RNA (Figure 3A,P value <.0001 in HRMVPCs group) and protein (Figure 3B,P value <.001 in HRMVPCs group) levels, suggesting that *BGN* expression in pericytes was more sensitive to hypoxia. The increased BGN expression under hypoxic stimulation in HRMVPCs was also confirmed by Western blot analysis of cell lysates (Figure 3C) and immunofluorescent staining (Figure 3D) of treated HRMVPCs. We also examined the expression of BGN in pericytes of the RA-raised control and OIR retina at P17. Immunofluorescence staining of NG2 revealed the development of intermediate layer capillary plexus in the control retina at P17, with pericytes arranged almost equidistantly. In contrast, the pericytes was disordered in the OIR retina. Co-localization of BGN and NG2 was found in OIR retinal surface at the proliferative area (Figure 3E). Hence our findings suggested robust BGN upregulation in retinal pericytes in response to hypoxia during PA.

3.4 | The effect of BGN on pericyte activity

We proceeded to investigate the impact of BGN on pericytes by reducing its expression using *BGN*-specific targeting siRNA. *BGN* siRNA treatment successfully reduced *BGN* RNA and protein expression in pericytes (Figure 4A–C). EdU labeling revealed reduced HRMVPC cell proliferation

(Figure 4D). Reduced intracellular ROS concentration was found in pericytes treated with *BGN* siRNA, compared to those treated with control siRNA (Figure 4E). Furthermore, scratching analysis showed compromised wound healing capability of the *BGN* siRNA-treated HRMVPCs (Figure 4F).

The main function of pericytes is to communicate with and regulate endothelial cell activity,[36,37] we analyzed the effect of *BGN* knockdown in HRMVPCs on endothelial cells, using culture media (CM) collected from *BGN* siRNA- or control siRNA-treated HRMVPCs under hypoxic conditions (1% oxygen). We found decreased migration of the HRMEC cultured with CM obtained from *BGN* siRNA-treated pericytes, compared to cells cultured with CM obtained from control siRNA-treated pericytes under the same condition (Figure 4G). Tube formation was also decreased in the HRMEC cultured with CM obtained from *BGN* siRNA-treated pericytes compared to cells cultured with CM obtained from control siRNA-treated pericytes (Figure 4H). Collectively, these findings underscored the critical role of BGN on pericyte survival, proliferation and function as the supporter of endothelial cells.

3.5 | BGN stimulates pathological angiogenesis via the upregulation of CXCL12

To understand how pericyte-derived BGN participated in the PA, we conducted a comparative analysis of the gene expression profiles between HRMVPCs treated with *BGN*-specific siRNA and those treated with control siRNA under hypoxic conditions. Eighty-eight DEGs were identified (Figure 5A). The majority of the DEGs were associated with "cellular response to hypoxia," "angiogenesis," "positive regulation of vascular endothelial growth factor production," and "extracellular exosome" (Figure 5B). As expected, significant decrease in *BGN* and *HIF-1α* expression were found in *BGN* siRNA-treated pericytes (Figure 5A). We also found *CXCL12* as one of the most significantly downregulated
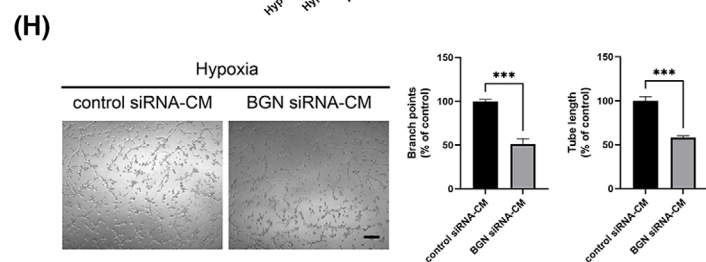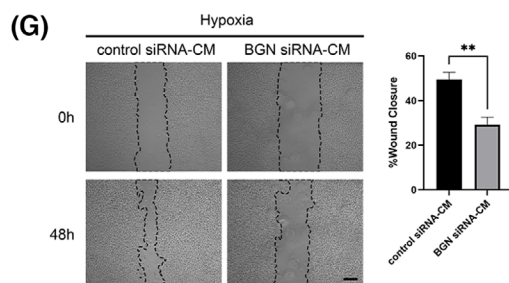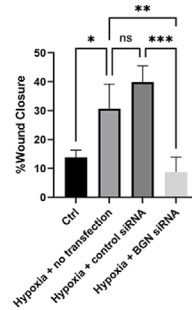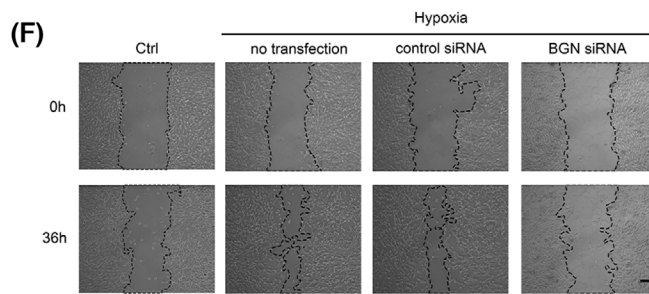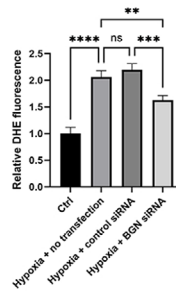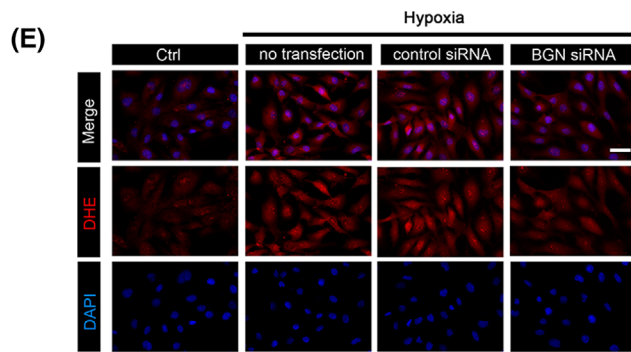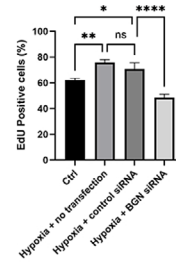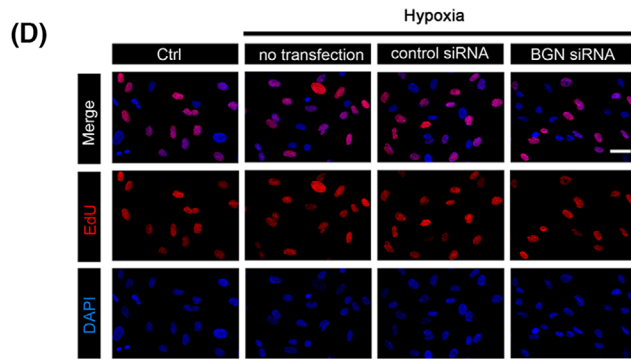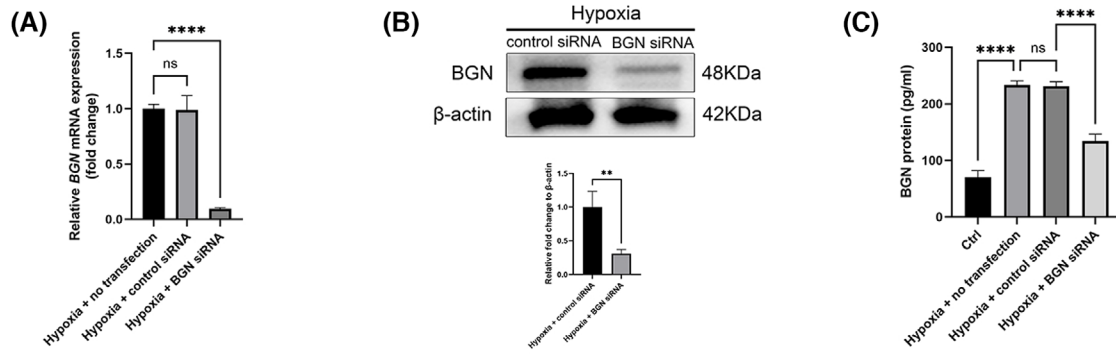
FIGURE 4 The effect of BGN on pericyte activity. (A–C) The effectiveness of *BGN*-specific siRNA in reducing BGN expression in HRMVPCs. Real-time PCR analysis (A), Western blot analysis (B), ELISA analysis of secreted BGN protein in cell culture medium (C) of HRMVPCs in indicated groups cultured in hypoxic conditions. For qPCR analysis, total RNA was extracted 24 h after transfection and the expression in no transfection group was set as 1. For Western blot and ELISA analysis, the samples were prepared 48 h after transfection. The average results of densitometric analysis is presented (below) using β-actin as loading control. Each assay was repeated 3–5 times using samples from different animals in each group. (D) EdU staining (red) in HRMVPCs of control, hypoxia, hypoxia plus control siRNA, and hypoxia plus *BGN* siRNA group shows the effect of BGN deficiency on HRMVPC cell proliferation. The nuclei were stained with DAPI (blue). The experiment was repeated in three different samples of each group and the ratio of positive cell number were quantified using ImageJ. Scale bar, 50 μm. (E) DHE staining (red) of HRMVPCs in the above-mentioned groups demonstrates the effect of BGN deficiency on HRMVPCs intracellular ROS level. The nuclei were stained with DAPI (blue). The experiment was repeated in 3 different samples of each group and the average fluorescent signals were quantified using ImageJ and photos taken under the same exposure conditions. Scale bar, 50 μm. (F and G). The effect of BGN deficiency on HRMVPCs (F) and HRMECs (G) migration capacity under hypoxia were analyzed by scratching assay. Cells were wounded with a 1 mL pipette tip and images of HRMVPCs were taken immediately after scratching and 36 h post-scratch while those of HRMECs were taken immediately after scratching and 48 h post-scratch. The experiments were repeated in 3–5 different samples of each group and two fields were calculated per sample. The wound closure ratio was quantified using the ImageJ software (right). For HRMEC migration analysis, the HRMECs were cultured with conditioned medium (CM) collected from HRMVPCs transfected *BGN* siRNA or control siRNA. Scale bar: 500 μm. (H) The effect of pericyte BGN deficiency on HRMECs tube formation capacity using Matrigel assay. HRMECs were cultured under hypoxia condition for 6 h in CM obtained from HRMVPCs as described above. The experiment was repeated in three different samples of each group and two fields were calculated per sample. The cumulative tube length and branch points were quantified using the ImageJ (right). The tube length and branch points in control siRNA-CM group was set as 1. Scale bar: 500 μm. Data are expressed as mean ± SD (*t* test). ns, not significant. *$p < .05$; **$p < .01$; ***$p < .001$; ****$p < .0001$.

angiogenesis-related genes in pericytes after *BGN* siRNA treatment (Figure 5A). The *BGN* siRNA-induced reduction of *CXCL12* and *HIF-1a* expression in hypoxic HRMVPCs was also confirmed at protein levels by Western blot and immunofluorescence analysis (Figure 5C–E). ELISA assays further confirmed the decreased CXCL12 concentration in the culture media (Figure 5F).

CXCL12 is one of the most potent chemokines in stimulating endothelial cell migration, tube formation and angiogenesis.[53,54] To test the causal relationship between BGN and CXCL12 on endothelial cell activity, we added recombinant CXCL12 protein to the medium of endothelial cells cultured with CM obtained from control siRNA- or *BGN* siRNA-treated pericytes, and analyzed wound healing and tube formation responses. The reintroduction of CXCL12 largely reversed the reduction in tube formation and the impaired wound healing in HRMECs (Figure 5G,H). Collectively, these results suggested that the proangiogenic effect of BGN was carried out via CXCL12 in vitro.

3.6 | Anti-CXCL12 and anti-CXCR4 treatment ameliorated pathological angiogenesis in vivo

Although *Cxcl12* expression was not significantly increased in P17 OIR retinas compared to RA-raised control retinas (Figure S4), we found significantly increased CXCL12 protein expression by Western blot analysis (Figure 6A,B) and immunofluorescent

staining (Figure S5) in P17 OIR retinas compared to controls. This is also consistent with higher expression of *Cxcr4* in P17 OIR retinas compared to controls (Figure 1D), which is the most well-known binding receptor to CXCL12.[55] Furthermore, *BGN* siRNA treatment successfully decreased *CXCL12* expression (Figure 6A,B). This was also accompanied by decreased expression of *HIF-1a* (Figure 6A,B). The results supported the regulatory role of BGN on *CXCL12* in the retina of OIR. Next, we administered LIT-927, a potent CXCL12 neutralizing agent,[56] and IT1t, a CXCR4 antagonist,[57] into the vitreous cavity of control (Figure S6) and OIR mice (Figure 6C) at P12, separately. Both treatments effectively diminished OIR-induced pathological neovascularization.

Finally, we analyzed the bulk RNA-sequencing data obtained from 20 neovascular proliferative membranes of patients with PDR and three controls (GSE102485) and found the upregulation of both *BGN* and *CXCL12* genes in PDR group (Figure 6D). Collectively, the finding supported the regulatory role of BGN on *CXCL12* expression during retinal pathological neovascularization.

4 | DISCUSSION

In this study, we showed that *Bgn* expression was significantly increased in the retina of OIR mice. This is in line with the reported increase in BGN cleavage products found in the vitreous of PDR patients.[35] We showed that the silencing of *Bgn* expression resulted in decreased retinal
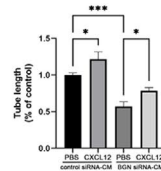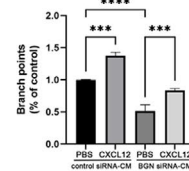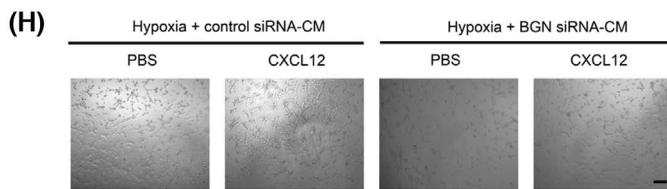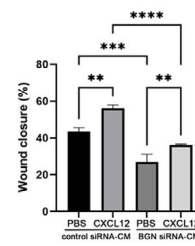
(A)

(B)

(C)

(D)

(E)

(F)

(G)

(H)
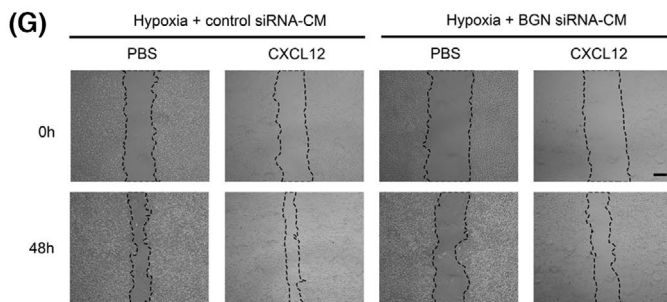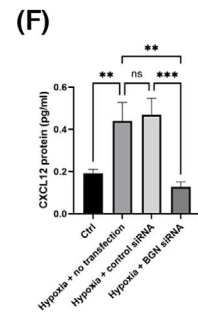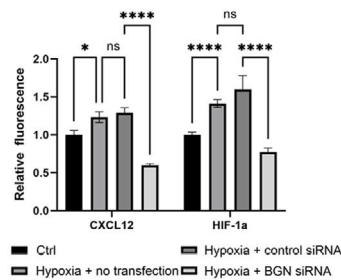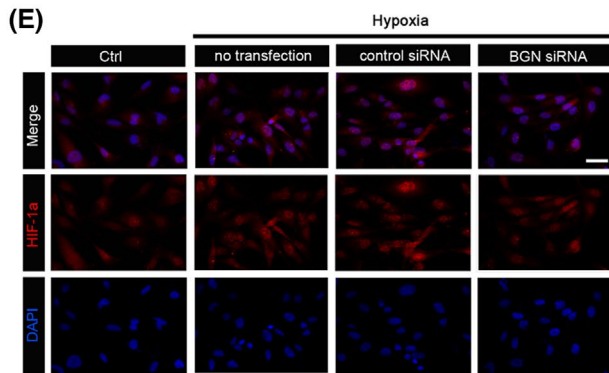
FIGURE 5 BGN stimulates pathological angiogenesis via the upregulation of CXCL12. (A) Volcano plot showing that the expression level of *CXCL12* is decreased in *BGN* siRNA- transfected HRMVPCs compared to those transfected with control siRNA in hypoxia for 24 h. The cut-off criteria were: |Fold change| >0.5 and adjusted *p*-value <.05 and marked by dotted lines. (B) The top 10 gene ontology terms related to biological process, cellular component and molecular function enriched by 88 DEGs. Terms of interest are marked in red. (C) 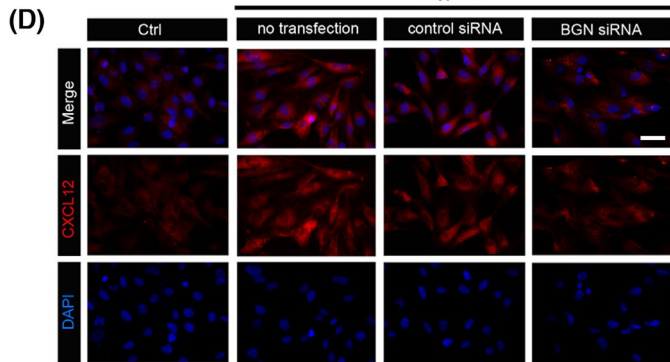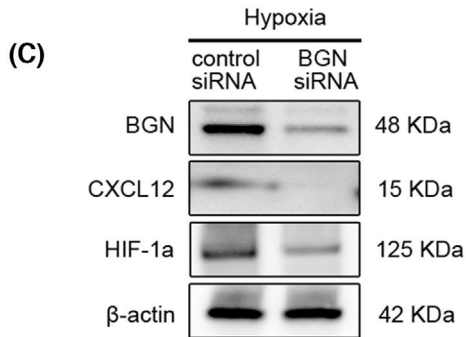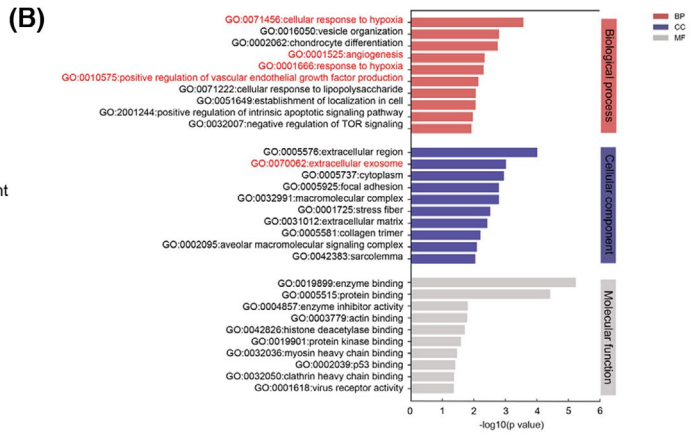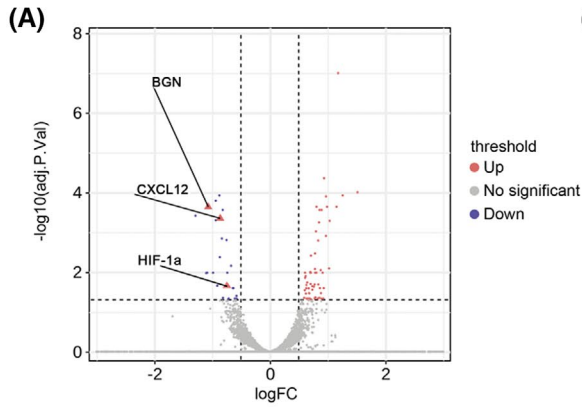Western blot analysis of BGN, CXCL12 and HIF-1a expression of HRMVPCs transfected with *BGN* siRNA as compared to those transfected with control siRNA in hypoxia for 48 h. The experiments were repeated using four different samples in each group. (D and E). Immunofluorescent staining of CXCL12 (D, red) and HIF-1a (E, red) in HRMVPCs of control, hypoxia, hypoxia plus control siRNA, and hypoxia plus *BGN* siRNA group. The nuclei were stained with DAPI (blue). The experiments were repeated in three different samples of each group and the fluorescent signals of were taken under the same exposure conditions and quantified using ImageJ. Scale bar, 50 μm. (F) CXCL12 protein level in the supernatant of HRMVPCs culture medium of the above-mentioned groups. The experiment was repeated in three different samples of each group. (G) The effect of reintroduction of rhCXCL12 on migration capacity of HRMECs. HRMECs were wounded with a 1 mL pipette tip and then cultured under hypoxia condition in CM collected from control siRNA- or *BGN* siRNA-treated HRMVPCs with or without reintroduction of rhCXCL12 for 48 h. Photographs were taken immediately and 48 h later. The experiment was repeated in six different samples of each group and two fields were calculated per sample. The wound closure ratio was quantified using ImageJ (right). Scale bar: 500 μm. (H) The effect of reintroduction of rhCXCL12 on tube formation capacity of HRMECs using Matrigel assay. HRMECs were cultured with CM collected from control siRNA- or *BGN* siRNA-treated HRMVPCs in a hypoxic condition with or without reintroduction of rhCXCL12 for 6 h. The experiment was repeated in 4 different samples of each group and two fields were calculated per sample. The cumulative tube length and branch points were quantified using the ImageJ and the tube length and branch points in control siRNA-CM group was set as 1 (right). Scale bar: 500 μm. Data are expressed as mean ± SD (*t* test). ns, not significant. *p<.05; **p<.01; ***p<.001; ****p<.0001.

neovascularization and improved revascularization in OIR mice, therefore extended the spectrum of BGN regulated angiogenesis to retinal PA. We further identified pericytes as a hypoxia-sensitive cellular source of BGN, and showed that BGN specifically upregulated *CXCL12* expression in pericytes, which acted as a mediator of the pro-angiogenic effect of BGN in OIR.

Studies on the proangiogenic role of BGN are mostly focused on endothelial cells, which showed a cell autonomous stimulation of endothelial cell proliferation, migration and sprouting.[31,32,34,58] Abnormal BGN expression is intricately linked to vasculogenesis or angiogenesis under injury-related conditions.[59–61] In this study, we demonstrated that the expression of *BGN* in pericytes of the retinal vessel was more sensitive to hypoxic stimulation than endothelial cells, therefore suggested that pericytes are another important cell source for BGN production during hypoxia-induced retinal angiogenesis. The production of BGN from retinal pericytes was first reported in bovine.[62] As indirect support of the importance of pericyte-derived BGN on PA, recent bulk and single-cell transcriptomic studies of cancer tissue revealed high *BGN* expression in cancer-associated fibroblast, a cell type which is similar to pericytes in origin and function in promoting angiogenesis.[63–65] Collectively, our results added to the repertoire of mechanisms by which pericytes regulate retinal microvascular remodeling.

Mechanistically, we showed that CXCL12 is one of the main effector molecules for pericyte-derived BGN. CXCL12 stimulates endothelial cell proliferation, branching and sprouting, VEGF secretion and endothelial progenitor cell chemotaxis.[54,66] Notably, we observed an

increase in CXCL12 protein expression, while *Cxcl12* levels did not show a corresponding rise in P17 OIR retinas. This discrepancy suggests that the upregulation of *Cxcl12* expression may have occurred at an earlier stage and returned to baseline by P17, whereas the elevated protein levels persisted. Given that CXCL12 binds to CXCR4, which is highly expressed in endothelial cells, we further investigated the implications of this interaction. Our findings revealed an increased expression of *Cxcr4* in the P17 OIR retina, and blocking the CXCL12/CXCR4 axis effectively abolished the pro-angiogenic effects of BGN under hypoxic conditions.

Evidence to support BGN regulated *CXCL12* expression in hypoxia-stimulated pericytes also came from the down-regulation of *HIF-1a* after *BGN* siRNA treatment, a known transcriptional factor for *CXCL12*. Hypoxia-induced *HIF-1a* expression was significantly downregulated by *BGN* siRNA treatment. BGN is known to bind to TLR 2 and 4.[19] It is conceivable that the BGN binding to TLR 2/4 stimulated the expression of *HIF-1a* through the activation of *NF-kB*.[31]

Additionally, the 3D interactions between pericytes and endothelial cells in the retinal vascular bed is essential for their functionality. The in vitro model used in this study may not capture the complexity of in vivo conditions. Future studies should employ 3D culture systems or co-culture models to better mimic the physiological environment and improve our understanding of pericyte-endothelial cell interactions.

In conclusion, our study demonstrated that BGN at the retinal surface is an important stimulator of PA, and it exerts the pro-angiogenic function via the upregulation of
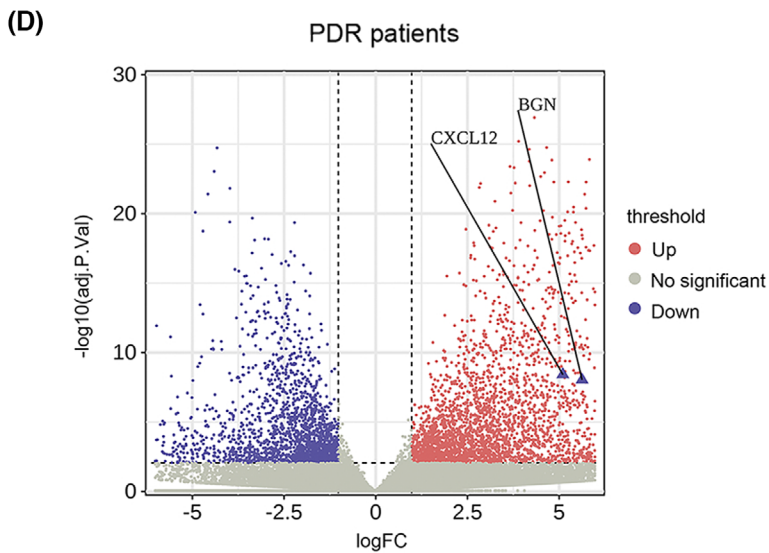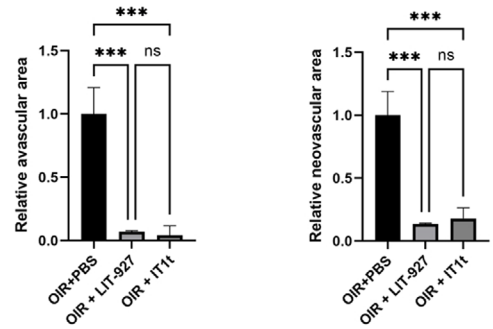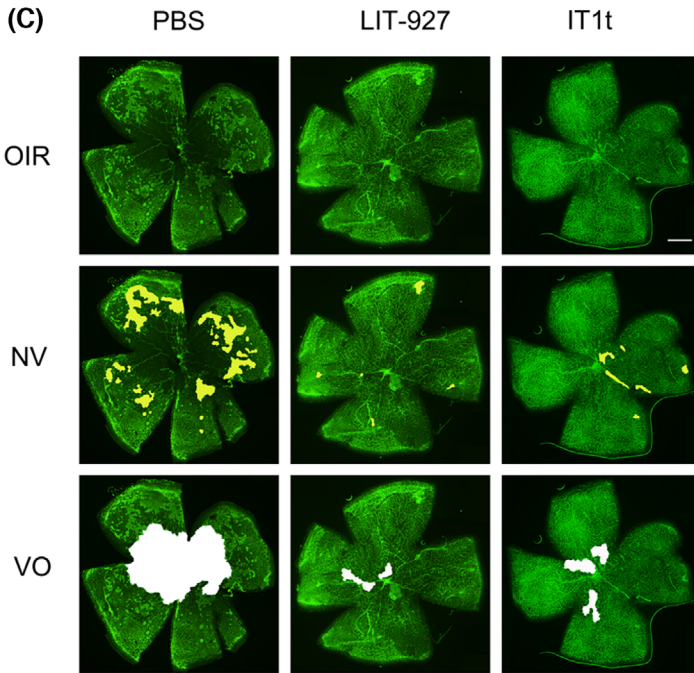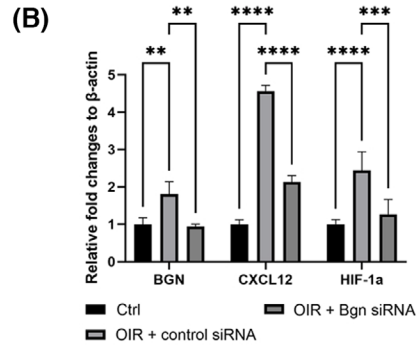
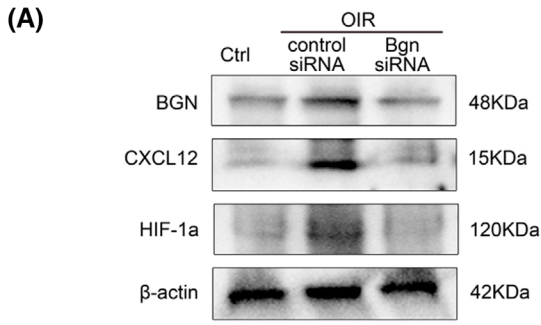**(A)**

(B)

(C)

(D)

FIGURE 6 Anti-CXCL12 and anti-CXCR4 treatment ameliorated pathologic angiogenesis in vivo. (A and B) Western blot analysis of BGN, CXCL12 and HIF-1a expression in P17 retinas of control, OIR treated with control siRNA, and OIR treated with *BGN* siRNA. The experiments were repeated on four different retinal total lysates in each group. The density of the bands was quantified using ImageJ and β-actin as internal control (B). (C) Immunofluorescent staining of IB4 on whole-mount of P17 OIR mice intravitreally injected with PBS, LIT-927 or IT1t at P12. The NV is marked in yellow, and the VO area is marked in white. The staining was performed on nine retinas of OIR mice. Quantification data were presented at the right. Scale bar: 500 μm. (D) Volcano plot showing the upregulation of *BGN* and *CXCL12* in 20 human neovascular proliferative membranes of PDR patients with PDR compared with three control samples without PDR based on bulk RNA-sequencing data (GSE102485). The cut-off criteria were: |Fold change| >0.5 and adjusted *p*-value <.05 and marked by dotted lines. Data are expressed as mean ± SD (*t* test). ns, not significant. **$p < .01$; ***$p < .001$; ****$p < .0001$.

CXCL12. We also showed that at least part of the increased BGN is originated from hypoxia-stimulated pericytes. Our study thus provided potential targets to control the growth of PA in retina.

AUTHOR CONTRIBUTIONS

Miaomiao Liu performed research, analyzed data, and wrote the paper; Ping Fei, Jing Li, and Peiquan Zhao conceived the project, designed research, and edited the manuscript; Huazhang Feng performed part of the experiments and helped wrote the paper; Yuan Yang and Xuerui Zhang helped recorded and analyzed data; Enguang Chen and Haodong Xiao performed part of the in vivo experiments; Jia Luo and Min Lin participated in the experiments and edited the manuscript; Jiawei Yin and Han Chen analyzed part of the data; Ruixue Mao and Xingping Zhu participated in the experiments and analyzed data.

DISCLOSURES

The authors declare that they have no conflict of interest.

DATA AVAILABILITY STATEMENT

The data supporting the findings of this study are available from the corresponding author upon request.

ETHICS STATEMENT

All animal experiments were approved by the Institutional Animal Care and Use Committee of Xinhua Hospital Affiliated to Shanghai Jiao Tong University School of Medicine.

ORCID

Miaomiao Liu https://orcid.org/0009-0004-9588-0692
Peiquan Zhao https://orcid.org/0000-0002-5092-9550
Huazhang Feng https://orcid.org/0009-0000-4693-8297
Xuerui Zhang https://orcid.org/0000-0002-1749-5391
Ping Fei https://orcid.org/0000-0001-7276-4630

REFERENCES

1. Folkman J. Angiogenesis in cancer, vascular, rheumatoid and other disease. *Nat Med*. 1995;1(1):27-31.
2. Sapieha P, Joyal JS, Rivera JC, et al. Retinopathy of prematurity: understanding ischemic retinal vasculopathies at an extreme of life. *J Clin Invest*. 2010;120(9):3022-3032.
3. Gariano RF, Gardner TW. Retinal angiogenesis in development and disease. *Nature*. 2005;438(7070):960-966.
4. Mettu PS, Allingham MJ, Cousins SW. Incomplete response to anti-VEGF therapy in neovascular AMD: exploring disease mechanisms and therapeutic opportunities. *Prog Retin Eye Res*. 2021;82:100906.
5. Levine SR, Sapieha P, Dutta S, Sun JK, Gardner TW. It is time for a moonshot to find "cures" for diabetic retinal disease. *Prog Retin Eye Res*. 2022;90:101051.
6. Tsai AS, Chou HD, Ling XC, et al. Assessment and management of retinopathy of prematurity in the era of anti-vascular endothelial growth factor (VEGF). *Prog Retin Eye Res*. 2022;88:101018.
7. Bressler SB, Liu D, Glassman AR, et al. Change in diabetic retinopathy through 2 years: secondary analysis of a randomized clinical trial comparing aflibercept, bevacizumab, and ranibizumab. *JAMA Ophthalmology*. 2017;135(6):558-568.
8. Stahl A, Krohne TU, Eter N, et al. Comparing alternative ranibizumab dosages for safety and efficacy in retinopathy of prematurity: a randomized clinical trial. *JAMA Pediatr*. 2018;172(3):278-286.
9. Muqit MM, Wakely L, Stanga PE, Henson DB, Ghanchi FD. Effects of conventional argon panretinal laser photocoagulation on retinal nerve fibre layer and driving visual fields in diabetic retinopathy. *Eye (Lond)*. 2010;24(7):1136-1142.

10. Nitkin CR, Bamat NA, Lagatta J, et al. Pulmonary hypertension in preterm infants treated with laser vs anti-vascular endothelial growth factor therapy for retinopathy of prematurity. *JAMA Ophthalmology*. 2022;140(11):1085-1094.

11. Fei P, Palenski TL, Wang S, et al. Thrombospondin-2 expression during retinal vascular development and neovascularization. *J Ocul Pharmacol Ther*. 2015;31(7):429-444.

12. Luo J, Zhao PQ, Chen HJ, Liu MM, He JQ, Fei P. Procollagen C-proteinase enhancer 1 promotes physiologic retinal angiogenesis via regulating the process of collagen. *Int J Ophthalmol*. 2022;15(6):868-875.

13. Xia FJ, Lyu J, Zhang X, Fei P, Zhao PQ. Early-onset neovascular inflammatory vitreoretinopathy due to two de novo CAPN5 mutations in Chinese patients: a case series. *Ocul Immunol Inflamm*. 2023;31(9):1777-1784.

14. Li J, He J, Zhang X, Li J, Zhao P, Fei P. TSP1 ameliorates age-related macular degeneration by regulating the STAT3-iNOS signaling pathway. *Exp Cell Res*. 2020;388(1):111811.

15. Scuruchi M, Potì F, Rodríguez-Carrio J, Campo GM, Mandraffino G. Biglycan and atherosclerosis: lessons from high cardiovascular risk conditions. *Biochim Biophys Acta Mol Cell Biol Lipids*. 2020;1865(2):158545.

16. Low SWY, Connor TB, Kassem IS, Costakos DM, Chaurasia SS. Small leucine-rich proteoglycans (SLRPs) in the retina. *Int J Mol Sci*. 2021;22(14):ijms22147293.

17. Keenan TD, Clark SJ, Unwin RD, Ridge LA, Day AJ, Bishop PN. Mapping the differential distribution of proteoglycan core proteins in the adult human retina, choroid, and sclera. *Invest Ophthalmol Vis Sci*. 2012;53(12):7528-7538.

18. Ali SA, Hosaka YZ, Uehara M. Spatiotemporal distribution of chondroitin sulfate proteoglycans in the developing mouse retina and optic nerve. *J Vet Med Sci*. 2011;73(1):13-18.

19. Schaefer L, Babelova A, Kiss E, et al. The matrix component biglycan is proinflammatory and signals through toll-like receptors 4 and 2 in macrophages. *J Clin Invest*. 2005;115(8):2223-2233.

20. Song R, Ao L, Zhao KS, et al. Soluble biglycan induces the production of ICAM-1 and MCP-1 in human aortic valve interstitial cells through TLR2/4 and the ERK1/2 pathway. *Inflamm Res*. 2014;63(9):703-710.

21. Babelova A, Moreth K, Tsalastra-Greul W, et al. Biglycan, a danger signal that activates the NLRP3 inflammasome via toll-like and P2X receptors. *J Biol Chem*. 2009;284(36):24035-24048.

22. Hoermann H, Krueger I, Maurus N, et al. The proteoglycan Biglycan modulates platelet adhesion and thrombus formation in a GPVI-dependent manner. *Int J Mol Sci*. 2021;22(22):ijms222212168.

23. Nastase MV, Young MF, Schaefer L. Biglycan: a multivalent proteoglycan providing structure and signals. *J Histochem Cytochem*. 2012;60(12):963-975.

24. Appunni S, Anand V, Khandelwal M, Gupta N, Rubens M, Sharma A. Small leucine rich proteoglycans (decorin, biglycan and lumican) in cancer. *Clinica Chimica Acta; International Journal of Clinical Chemistry*. 2019;491:1-7.

25. Xu T, Bianco P, Fisher LW, et al. Targeted disruption of the biglycan gene leads to an osteoporosis-like phenotype in mice. *Nat Genet*. 1998;20(1):78-82.

26. Westermann D, Mersmann J, Melchior A, et al. Biglycan is required for adaptive remodeling after myocardial infarction. *Circulation*. 2008;117(10):1269-1276.

27. Yu M, He X, Song X, et al. Biglycan promotes hepatic fibrosis through activating heat shock protein 47. *Liver Int*. 2023;43(2):500-512.

28. Roedig H, Nastase MV, Wygrecka M, Schaefer L. Breaking down chronic inflammatory diseases: the role of biglycan in promoting a switch between inflammation and autophagy. *FEBS J*. 2019;286(15):2965-2979.

29. Pinto F, Santos-Ferreira L, Pinto MT, Gomes C, Reis CA. The extracellular small leucine-rich proteoglycan Biglycan is a key player in gastric cancer aggressiveness. *Cancer*. 2021;13(6):13061330.

30. Manupati K, Paul R, Hao M, et al. Biglycan promotes cancer stem cell properties, NFκB signaling and metastatic potential in breast cancer cells. *Cancers (Basel)*. 2022;14(2):14020455.

31. Hu L, Zang MD, Wang HX, et al. Biglycan stimulates VEGF expression in endothelial cells by activating the TLR signaling pathway. *Mol Oncol*. 2016;10(9):1473-1484.

32. Chui A, Gunatillake T, Brennecke SP, et al. Expression of Biglycan in first trimester chorionic villous sampling placental samples and altered function in telomerase-immortalized microvascular endothelial cells. *Arterioscler Thromb Vasc Biol*. 2017;37(6):1168-1179.

33. Myren M, Kirby DJ, Noonan ML, et al. Biglycan potentially regulates angiogenesis during fracture repair by altering expression and function of endostatin. *Matrix Biology*. 2016;52-54:141-150.

34. Yamamoto K, Ohga N, Hida Y, et al. Biglycan is a specific marker and an autocrine angiogenic factor of tumour endothelial cells. *Br J Cancer*. 2012;106(6):1214-1223.

35. Abu El-Asrar AM, Nawaz MI, Allegaert E, et al. Differential expression and localization of ADAMTS proteinases in proliferative diabetic retinopathy. *Molecules (Basel, Switzerland)*. 2022;27(18):27185977.

36. Armulik A, Genové G, Betsholtz C. Pericytes: developmental, physiological, and pathological perspectives, problems, and promises. *Dev Cell*. 2011;21(2):193-215.

37. Caporarello N, D'Angeli F, Cambria MT, et al. Pericytes in microvessels: from "mural" function to brain and retina regeneration. *Int J Mol Sci*. 2019;20(24):ijms20246351.

38. Huijbers EJ, van Beijnum JR, Thijssen VL, Sabrkhany S, Nowak-Sliwinska P, Griffioen AW. Role of the tumor stroma in resistance to anti-angiogenic therapy. *Drug Resist Updat*. 2016;25:26-37.

39. Huang H. Pericyte-endothelial interactions in the retinal microvasculature. *Int J Mol Sci*. 2020;21(19):ijms21197413.

40. Sweeney MD, Ayyadurai S, Zlokovic BV. Pericytes of the neurovascular unit: key functions and signaling pathways. *Nat Neurosci*. 2016;19(6):771-783.

41. Alarcon-Martinez L, Yemisci M, Dalkara T. Pericyte morphology and function. *Histol Histopathol*. 2021;36(6):633-643.

42. Cai W, Liu H, Zhao J, et al. Pericytes in brain injury and repair after ischemic stroke. *Transl Stroke Res*. 2017;8(2):107-121.

43. Kale S, Hanai J, Chan B, et al. Microarray analysis of in vitro pericyte differentiation reveals an angiogenic program of gene expression. *FASEB J*. 2005;19(2):270-271.

44. Carlsson R, Enström A, Paul G. Molecular regulation of the response of brain pericytes to hypoxia. *Int J Mol Sci*. 2023;24(6):ijms24065671.

45. Enström A, Carlsson R, Özen I, Paul G. RGS5: a novel role as a hypoxia-responsive protein that suppresses chemokinetic

and chemotactic migration in brain pericytes. *Biol Open*. 2022;11(10):bio059371.

46. Orlich MM, Diéguez-Hurtado R, Muehlfriedel R, et al. Mural cell SRF controls pericyte migration, vessel patterning and blood flow. *Circ Res*. 2022;131(4):308-327.

47. Motegi S, Leitner WW, Lu M, et al. Pericyte-derived MFG-E8 regulates pathologic angiogenesis. *Arterioscler Thromb Vasc Biol*. 2011;31(9):2024-2034.

48. Dubrac A, Künzel SE, Künzel SH, et al. NCK-dependent pericyte migration promotes pathological neovascularization in ischemic retinopathy. *Nat Commun*. 2018;9(1):3463.

49. Zhou W, Zhou Y, He J, Rao Y, Fei P, Li J. TREM2 deficiency in microglia accelerates photoreceptor cell death and immune cell infiltration following retinal detachment. *Cell Death Dis*. 2023;14(3):219.

50. Maurya M, Liu CH, Bora K, et al. Animal models of retinopathy of prematurity: advances and metabolic regulators. *Biomedicine*. 2024;12(9):12091937.

51. Gu X, Samuel S, El-Shabrawey M, et al. Effects of sustained hyperoxia on revascularization in experimental retinopathy of prematurity. *Invest Ophthalmol Vis Sci*. 2002;43(2):496-502.

52. Armulik A, Abramsson A, Betsholtz C. Endothelial/pericyte interactions. *Circ Res*. 2005;97(6):512-523.

53. Shi Y, Riese DJ 2nd, Shen J. The role of the CXCL12/CXCR4/CXCR7 chemokine Axis in cancer. *Front Pharmacol*. 2020;11:574667.

54. Salcedo R, Oppenheim JJ. Role of chemokines in angiogenesis: CXCL12/SDF-1 and CXCR4 interaction, a key regulator of endothelial cell responses. *Microcirculation*. 2003;10(3–4):359-370.

55. Sanchis-Pascual D, Del Olmo-García MI, Prado-Wohlwend S, et al. CXCR4: from signaling to clinical applications in neuroendocrine neoplasms. *Cancers (Basel)*. 2024;16(10):16101799.

56. Regenass P, Abboud D, Daubeuf F, et al. Discovery of a locally and orally active CXCL12 Neutraligand (LIT-927) with anti-inflammatory effect in a murine model of allergic airway Hypereosinophilia. *J Med Chem*. 2018;61(17):7671-7686.

57. Wu B, Chien EY, Mol CD, et al. Structures of the CXCR4 chemokine GPCR with small-molecule and cyclic peptide antagonists. *Science*. 2010;330(6007):1066-1071.

58. Gubbiotti MA, Buraschi S, Kapoor A, Iozzo RV. Proteoglycan signaling in tumor angiogenesis and endothelial cell autophagy. *Semin Cancer Biol*. 2020;62:1-8.

59. Wight TN. A role for proteoglycans in vascular disease. *Matrix Biol*. 2018;71-72:396-420.

60. Zeng X, Chen J, Miller YI, Javaherian K, Moulton KS. Endostatin binds biglycan and LDL and interferes with LDL retention to the subendothelial matrix during atherosclerosis. *J Lipid Res*. 2005;46(9):1849-1859.

61. Heegaard AM, Corsi A, Danielsen CC, et al. Biglycan deficiency causes spontaneous aortic dissection and rupture in mice. *Circulation*. 2007;115(21):2731-2738.

62. Kaji T, Sakurai S, Yamamoto C, et al. Characterization of chondroitin/dermatan sulfate proteoglycans synthesized by bovine retinal pericytes in culture. *Biol Pharm Bull*. 2004;27(11):1763-1768.

63. Zhou Y, Bian S, Zhou X, et al. Single-cell multiomics sequencing reveals prevalent genomic alterations in tumor stromal cells of human colorectal cancer. *Cancer Cell*. 2020;38(6):818-828.e5.

64. He Z, Lin J, Chen C, et al. Identification of BGN and THBS2 as metastasis-specific biomarkers and poor survival key regulators in human colon cancer by integrated analysis. *Clin Transl Med*. 2022;12(11):e973.

65. Zheng S, Liang JY, Tang Y, et al. Dissecting the role of cancer-associated fibroblast-derived biglycan as a potential therapeutic target in immunotherapy resistance: a tumor bulk and single-cell transcriptomic study. *Clin Transl Med*. 2023;13(2):e1189.

66. Teicher BA, Fricker SP. CXCL12 (SDF-1)/CXCR4 pathway in cancer. *Clin Cancer Res*. 2010;16(11):2927-2931.

SUPPORTING INFORMATION

Additional supporting information can be found online in the Supporting Information section at the end of this article.